Informatics in Medicine Unlocked 15 (2019) 100183

Contents lists available at ScienceDirect

Informatics in Medicine Unlocked

journal homepage: www.elsevier.com/locate/imu

Robust medical image compression based on wavelet transform and vector quantization

Paul Nii Tackie Ammah, Ebenezer Owusu*

University of Ghana, Department of Computer Science, Box LG 163, Legon, Accra, Ghana

ARTICLE INFO

Keywords:
Medical image
Compression
DWT
VQ
Huffman coding

ABSTRACT

Medical imaging, such as Magnetic Resonance Imaging (MRI), Computed Tomography (CT), and Ultrasound, serves as a precursor for determining a patient's expedition towards therapeutics or surgery. The rising pervasiveness of chronic illnesses worldwide has resulted in a great increase in the number of diagnostic imaging techniques being executed annually. This, in turn, has given rise to more advanced imaging technologies and software to expedite accurate diagnosis. For the purposes of patient medical history, these images are stored for very long periods. Also, future research and medical developments renders such records very sensitive, emphasizing their need to be stored. Storing, however, poses a great challenge since there is limited storage capacity to preserve these ever growing medical images. Any technology that improves medical image compression is welcome, since indirectly, it also promotes applications such as telemedicine that require fewer bits to transmit imagery over a computer network. In this study is proposed a DWT-VQ (Discrete Wavelet Transform – Vector Quantization) technique to compress images, and to preserve their perceptual quality at a medically tolerant level. In this hybrid technique, speckle and salt and pepper noises in ultrasound imagery are significantly reduced. If the image is not ultrasound, the process has a negligible effect, but the edge is preserved. The images are then filtered using DWT. A threshold approach is applied to generate coefficients by efficient means. The result is then vector quantized. Finally, the quantized coefficients are Huffman encoded. The resulting bits that represent the compressed image are then stored, and retrieved when needed. The result of the proposed technique is promising, as it outperforms other recent techniques.

1. Introduction

Current studies have reported that the use of diagnostic imaging has skyrocketed in the last two decades [1]. For instance, in the US, a research conducted by Smith-Bindman et al. [2] in 2008 reported that imaging with CT doubled, and imaging with MRI tripled. This development is the result of rapid advancement of hardware and software to aid in the imaging system. Furthermore, the change from analog to digital systems offers more accurate, quicker, and stress-free imaging growth. All of these factors have contributed immensely to imaging collection; hence petabytes of these image types are obtained yearly across the world. The image acquisition technology is carried out through X-Ray, Ultrasound, MRI/fMRI (functional Magnetic Resonance Image), Nuclear Medicine, PET (Positron Emission Tomography), CT (Computerized Tomography) [3], and DXA (dual energy X-ray absorptiometry). The need to store, share, and retrieve these images in their original form have contributed to the picture archiving and communication system (PACS) which is a medical imaging technology that offers inexpensive storage and useful access to images from several sources. Unfortunately, the large pixel sizes of these images put a serious constraint on the capacity of storage devices [4–6]. For instance, a typical matrix size for an MRI is 512 by 512, with a pixel depth of 16 bits [7]. A health organization that generates hundreds of such images weekly will require several megabytes of storage space. Over a year, the amount of storage required grows to several gigabytes. This development leads to several terabytes of storage required yearly. In addition to this, a bandwidth of 56 kbps transmission of an MRI will require 12–15 min; and for a very low bandwidth, such as 14.4 kbps, this could take almost an hour to transmit [8].

Many techniques have been advanced to compress these images, but

* Corresponding author.
E-mail address: ebeowusu@ug.edu.gh (E. Owusu).

https://doi.org/10.1016/j.imu.2019.100183
Received 13 December 2018; Received in revised form 9 April 2019; Accepted 13 April 2019
Available online 16 April 2019

the most sought-after innovation is the hybrid imaging technique of which the wavelet transform (DWT) and vector quantization (VQ), both of which are lossy [9], are the most preferred.

In numerical and functional analyses, a DWT is any wavelet transform whose wavelets are discretely sampled and is developed for processing discrete-time signals [10,11]. Unlike the case of the Discrete Cosine Transform (DCT) which is based on cosine functions, the basis of DWT can be composed of any function that satisfies the requirements of multiresolution analysis [12].

The basis of compression algorithms is to take an input X and generate a representation $X^{'}$ that should require fewer bits for representation. This is followed by a reconstruction algorithm that operates on the compressed representation X' to generate the reconstruction Y [13].

The emergence of wavelet transforms has encouraged the exploration of its application areas. The DWT provides a set of wavelet coefficients at different resolution levels that exhibit different statistical characteristics [14]. To design a quantizer for each set through the VQ technique, the bit rate can be significantly reduced without degrading the quality. However, quantization results in the loss of signal quality. According to Shannon [15], the dimension of a chosen vector greatly affects the performance of quantization. Vectors of larger dimension produce better quality as compared to vectors of smaller dimension.

For that reason, the aim of this study is to propose a hybrid technique based on Discrete Wavelet Transforms and Vector Quantization to compress medical images in an efficient manner to achieve high compression ratios and high quality. The study explores the use of a threshold after generation of DWT coefficients before they are quantized. Different DWT levels are also employed to assess its performance. The rest of the study is presented as follows: section 2 describes some related work. Section 3 describes the proposed technique. The result of the study is discussed in section 4, and finally, the conclusion is drawn in section 5.

2. Related work

Wavelet transforms and vector quantization are hotbed research areas in signals processing. The use of techniques such as DWT and VQ in compression is not a new development; several researchers have used them in different ways to build compression systems. For example, Tejas et al. [16] proposed a hybrid algorithm that employs DWT and VQ as the main techniques in the compression of images. In that study, an image is transformed after which the resulting coefficients are preprocessed and finally vector quantized. They applied DWT transform on the original image and obtained four sub-bands of the original image, and the mean of each block was computed. Then they subtracted the mean of the block from each element of that block to obtain the difference matrix. Finally, vector quantization was applied to this difference matrix. The result showed a better compression ratio when compared with the same technique without the preprocessing stage, but the margin of error was still too wide. Another drawback of the study is that the mean of each block has to be transported along with the codebook to the decoder, making the overall size of the resulting data twice the quantized data.

Aree and Jamal [17] also proposed a hybrid transform scheme for medical image compression using the DWT and Discrete Cosine Transform (DCT). They converted the image from RGB to YCbCr and then applied a forward DWT. They then divided each HL and LH subband into 8 × 8 blocks and converted to the frequency domain using 2D forward DCT. The resulting DCT coefficients were quantized using a luminance quantization matrix. The proposed algorithm was then applied to MRI medical images with two different sizes, brain (256 × 256) and pulmonary (512 × 512). However, one major weakness of using a DCT is the blocking artifacts that are evident in the reconstructed image. This severely damages the diagnostic content of the medical image.

The contourlet transform, an extension of the wavelet, together with Huffman coding has also been proposed by Janet et al. [18] in their effort to compress medical images losslessly. The input to their proposed system is a grayscale image. In this method, a 2-dimensional contourlet transform is applied to the input medical image and the image is split into 8 sub-bands. A global thresholding and Huffman encoding are then applied to the lower frequency sub-bands and the compression percentage is calculated. The finding is admirable, but an introduction of a vector quantization technique before Huffman encoding resulted in less bit representation of the compressed image.

3. Proposed method

In this technique, images are filtered at the preprocessing stage to remove speckle and salt and pepper noises in ultrasound imaging, since such images are inevitably affected [19]. If the image is not ultrasound it has a negligible effect, but edge preservation is achieved in all situations since it is a crucial step in all medical image diagnosis. The images are then filtered using DWT. A threshold is applied to the generated coefficients with the effect that coefficients that fall below that threshold are replaced by zeroes. The result is then vectored quantized. Finally, the quantized coefficients are Huffman encoded. Fig. 1 summarizes the process. The resulting bits that represent the compressed image are then stored or transmitted.

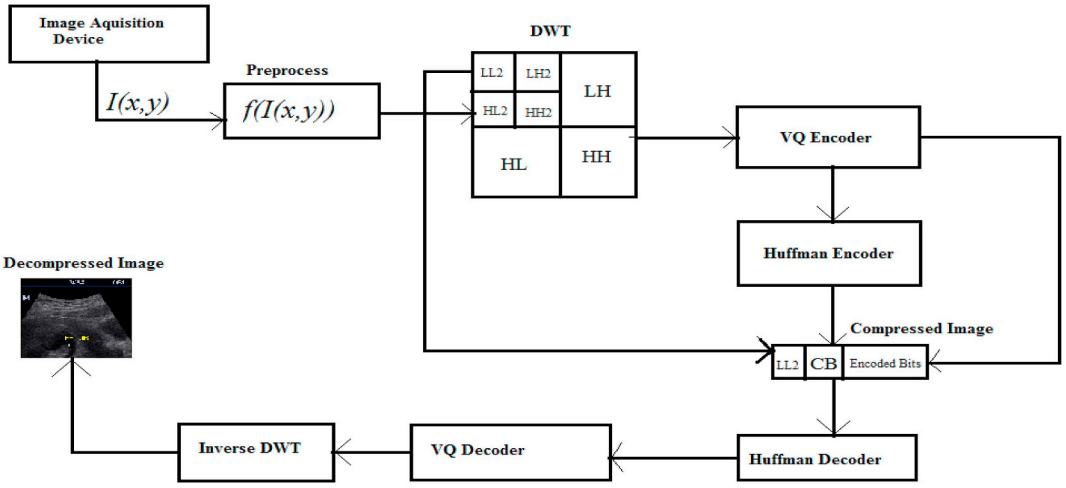

Fig. 1. Proposed model overview.

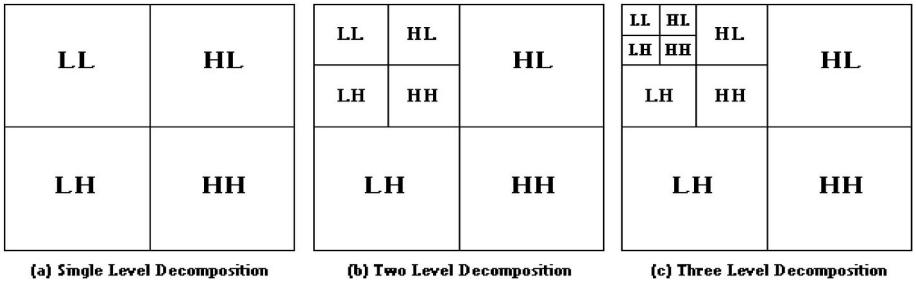

Fig. 2. Sub-band partitioning of image after DWT.

3.1. Image preprocessing

Medical images are corrupted by various types of noises such as salt and pepper and speckle [20]. In this study, noise was dealt with via a median filter [21] because of its advantage over edge preserving.

We chose an $n \times n$ window, where $n = 3$ represents the window size. Then each pixel in the $n \times n$ window was represented by Eq. (1), where x represents the position of the pixel along the rows and y corresponds to the columns

$$I'(x, y) = f(I(x, y)) \tag{1}$$

Where f is the median filter.

3.2. Wavelet coefficients

The filtered image is taken through multiple levels of discrete wavelet decomposition. Multilevel wavelet decomposition presents information about frequency modules, and enhances the information about the image for further dispensation. Also, it provides the means to achieve better reconstruction after compression, since the successive levels contain more useful information and less noise.

A 2D image is treated using a one-dimensional approach since it is faster and more efficient. The rows and the columns are then decomposed. The transformation is achieved by convolving the rows and columns of the 2D image with filters. The Daubechies 9/7 filter is used because of its ability to produce a high number of zeroes or vanishing moments. A test for two scenarios is then conducted as follows:

TEST CASE 1: Two-Level Decomposition of Image.

- STEP 1: Apply a DWT transform on the filtered image to generate four sub-bands: LL, LH, HL, and HH.
- STEP 2: Transform the LL block from the first operation to obtain the sub-bands for the second level.

TEST CASE 2: Three Level Decomposition of Image.

- STEP 1: Apply DWT transform on the filtered image to get four sub-bands; LL, LH, HL, and HH. The most detailed sub-band is the LL sub-band.
- STEP 2: Transform the resulting sub-band LL again to gain a new set of sub-bands whose LL sub-band is also transformed. This ensures that the image goes through three levels of decomposition.

At the end of this process, 7 sub-bands are obtained (three from the first level of decomposition and four from the second level of decomposition) for the first scenario and 10 different sub-bands for the second scenario (3 of which represent the LH, HL, HH of the first level of decomposition, another 3 representing the LH, HL, HH of the second level of decomposition and the remaining four sub-bands that of the final decomposition). The coefficients that fall below a certain threshold are discarded by replacing them with zero values. The approach used by Sarah et al. [22] to determine results over large samples of image data was used. The threshold value is determined by Eq. (2).

$$t = \frac{\theta(W(x, y))}{4 \times \theta(x, y)} \tag{2}$$

Where t is the threshold, $W(x, y)$ is the wavelet coefficients, x and y are the dimensions of the image and θ is a function that gives a measure of the coefficients generated. The sub-band partition of the image is shown in Fig. 2.

3.3. Vector quantization

VQ is applied to all of the resulting coefficients from the previous step, except the LL sub-band which contains the most significant details for reconstruction. Several enhancements have been made to reduce the computation time in generating the codebook. In this study, the approach used is the tree-structured vector quantization method, since it is faster and ensures that the reconstructed image is not severely distorted while reducing time. We employed the k-means algorithm, and it is assumed that the desired codebook size is a power of 2. To exploit the many zeroes generated by using the threshold approach, a default codeword is injected into the codebook. The algorithm is advanced as follows:

- STEP 1: Load the image coefficients to be quantized.
  From the previous step, where a two-level decomposition is conducted, the coefficients consisted of the following different sub-bands:
  Three sub-bands from the first-level (the LH, HL or HH), three sub-bands (the LH, HL, and HH) from the second-level. The LL sub-band of the second-level is omitted.
  For the second approach where a three-level decomposition is performed, the entirety of the resulting coefficients excluding the LL sub-band from the third-level of decomposition is loaded.
- STEP 2: Break up the image into non-overlapping blocks or vectors of the desired size. The block sizes used range from a 3×3 to a 9×9 (only odd window sizes are considered). This is done to investigate the performance on quality, and also compression achieved by varying the block sizes.
- STEP 3: Find the centroid for the entire set of vectors generated from the previous step.
- STEP 4: Split each centroid into two centroids, x, and y, and allow a small offset to have a small normal and random direction.
- STEP 5: Assign each data to a centroid to obtain separate groups. The groups from here onwards are treated separately.
- STEP 6: Find the centroids of the clusters generated.
- STEP 7: Calculate the total distance using the square Euclidean distance formula and compare to the desired distortion value. If the

number of centroids is smaller than desired, go to STEP 4, otherwise continue. Else if the distortion is higher than the maximum allowed, then move to STEP 5.

- STEP 8: If the number of centroids is larger than required, discard the centroid with the highest distortion or the lowest population. Go to STEP 3 and terminate.

The algorithm is fast, since computations are done on data sets that grow smaller, while ensuring that the vectors in each group are closely related to the centroids generated. Now we continue to encode the image coefficients with the generated codebook. The VQ encoder uses the codebook to encode the original DWT coefficients. For each non-overlapping block of the image coefficient, the encoder replaces it with an index of the codeword from the codebook with the lowest distortion rate. This is possible only after the squared Euclidean distance has been calculated for each codeword with the block to be quantized. The resulting data, which are sets of indexes, is a compressed form of the original coefficients generated by the DWT. The vector quantization operation is represented in Fig. 3.

3.4. Coding of image

The compressed image is reduced in bit size using the Huffman coding system. To ensure accurate decoding, the encoded sequence along with their code is used by the decoder to successfully recover the original data. To restore the image, the compressed image goes through a reverse of the compression process. The Huffman encoded data is first decoded to recover the indexes. The set of indexes is then passed to the VQ decoded along with the codebook for effective reconstruction of the data. The decoder now uses the indexes to lookup the code-word from the codebook to reform the wavelet coefficients. The LL block is then appended to the data. Once again in the approach where we discarded two of the sub-bands, the data is then padded with zeroes to make up for the two sub-bands that were discarded during the compression of the image. Finally, an inverse DWT is performed to retrieve the image. The restored image is of the same size as the original image.

3.5. Compression metrics

The compression ratio (*CR*), which is the ratio of the size of the original image by the size of the compressed image represented by Eq. (3), is used to evaluate the degree of compression of the original image

$$CR = \frac{I(x, y)}{I'(x, y)} \tag{3}$$

Where $I(x, y)$is the original image, $I'(x, y)$ is the compressed image, and x, y are the dimensions of the image.

The Peak Signal to Noise Ratio (PSNR) is the metric used to determine the quality of reconstruction in any compression method [23,24]. For a considerably good quality image reconstruction, the Peak Signal to Noise Ratio (PSNR) is large. The value of the PNSR is computed as:

$$PNSR = 10 \log_{10} \frac{255^2}{MSE} \tag{4}$$

$$MSE = \frac{1}{M * N} \sum_{x=1}^{M} \sum_{y=1}^{N} \left(I(x, y) - I'(x, y)\right)^2 \tag{5}$$

Where the value '255' signifies the 8-bit images for grayscale.Where M and N are dimensions of the image, and *MSE* is the Mean Squared Error.

Another index used is the Structural Similarity Index (SSIM) [25]. The SSIM is a perceptual metric that quantifies image quality degradation caused by processing such as data compression or by losses in data transmission. It is devised to advance on traditional metrics that proves to be incoherent with human eye perception. It is computed on various windows of an image. The measure between two windows x and y of common size $M \times N$ for two images can be formulated as the product of two partial indices S_L and S_V

$$SSIM = \left[\frac{2\mu_x\mu_y}{\mu_x^2 + \mu_y^2}\right] \times \left[\frac{2\sigma_x\sigma_y}{\sigma_x^2 + \sigma_y^2}\right] \times \left[\frac{\sigma_{xy}}{\sigma_x\sigma_y}\right]$$

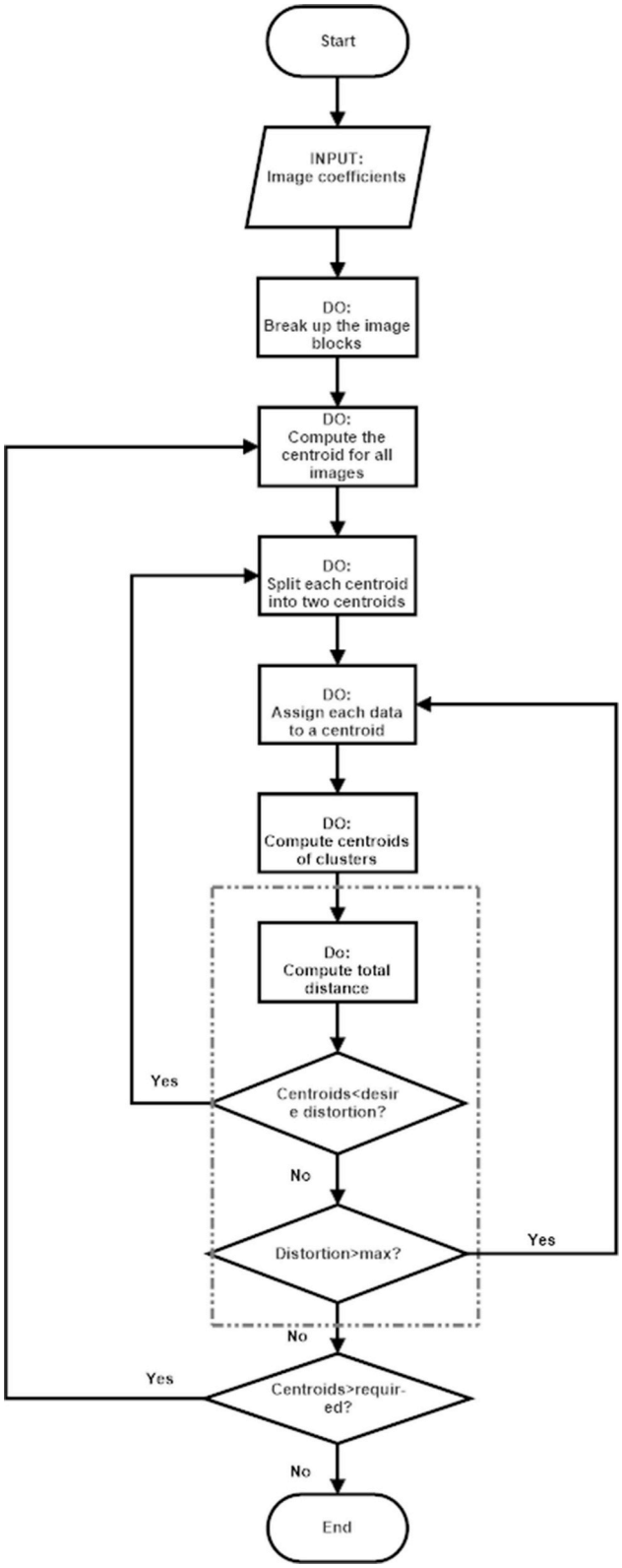

Fig. 3. Vector quantization operation.

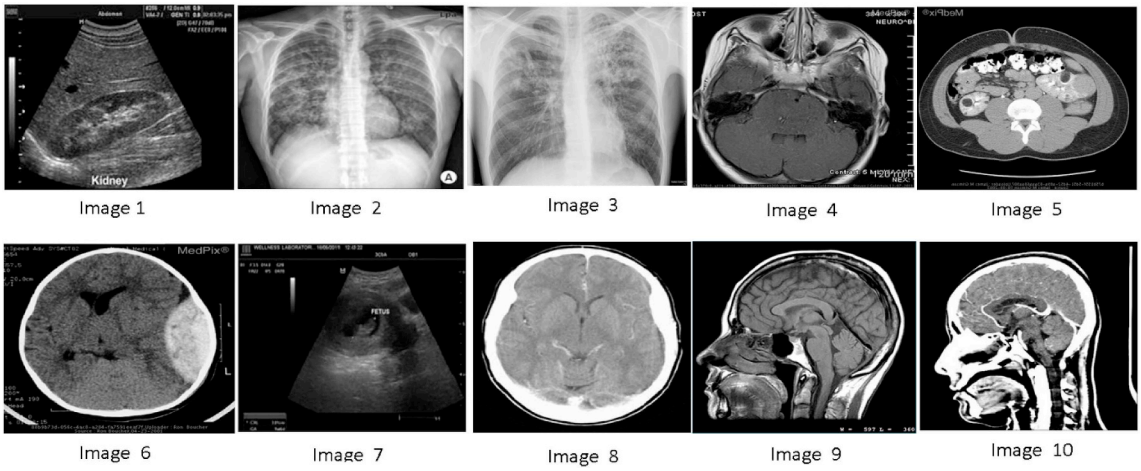

Fig. 4. Sample Original images (Image 1- Image 10).

$$SSIM = \left[\frac{2\mu_x\mu_y}{\mu_x^2+\mu_y^2}\right]\times\left[\frac{2\sigma_{xy}}{\sigma_x^2+\sigma_y^2}\right]$$

$$SSIM = S_L S_V \tag{6}$$

The index S_L contains the luminance and S_V contains the local covariance. The symbols μ and σ represent mean and standard deviation, respectively, computed by:

$$\mu_x = \frac{1}{K}\sum_{i=1}^{K} x_i \;\mu_y = \frac{1}{K}\sum_{i=1}^{K} y_i \tag{7}$$

$$\sigma_x = \left\{\frac{1}{K-1}\sum_{i-1}^{K}(x_i-\mu_x)^2\right\}^{1/2},\ \sigma_y = \left\{\frac{1}{K-1}\sum_{i-1}^{K}(y_i-\mu_y)^2\right\}^{1/2} \tag{8}$$

4. Results and discussion

4.1. Preprocessing phase

At this level, we evaluated the effect of compression on various window sizes. A graph of the performance for each window size is plotted. From Fig. 5, it is realized that the [3 × 3] window size generates an improved PSNR, which suggests that the filtered image is of higher quality (possible errors have been smoothened out, while the edges have been preserved). Increasing the window size increases the chances of obtaining a median, which is a wrong representation of the actual pixel of interest. Thus, the best groups of pixels for consideration in a median filter are the immediate pixels surrounding the pixel being processed. Fig. 4 shows sample tested original images, and Table 1 shows the PSNR and RMSE of the image after preprocessing using the [3 × 3] window size.

Table 1
Summary results from preprocessing phase.

IMAGE	PSNR (dB)	RMSE
Image 1	30.6818	0.4669
Image 2	34.1269	0.3140
Image 3	30.7759	0.4618
Image 4	32.3765	0.3841
Image 5	37.9788	0.2015
Image 6	35.3118	0.4289
Image 7	34.2190	0.4150
Image 8	34.6872	0.3618
Image 9	33.3791	0.3872
Image 10	31.8878	0.2411

Fig. 5(a–d) presents a pictorial view of two of the images before and after preprocessing. The window sizes of the images are3 × 3. Fig. 5(a) is corrupted with speckle noise, but the image is denoised after the

(a)

Fig. 5a. Original image contains speckle noise.

(b)

Fig. 5b. Filtered image removes the speckle noise.

processing. Fig. 5(b) shows the filtered image. Fig. 5(d) is not corrupted by noise, but the perceptual quality is retained after processing.

Fig. 6(a, b, c) shows plots of PSNR, RMSE and Time against the window size.

Fig. 5 (a) shows how the image degrades in quality as the window size for the median filter is increased. From the graph, it can be inferred that a window size of 3×3 is best to retain quality. In Fig. 5 (b) it can be noted that the error associated with a window size of 3×3 is minimal. This hence favors the application of the 3×3 window to the

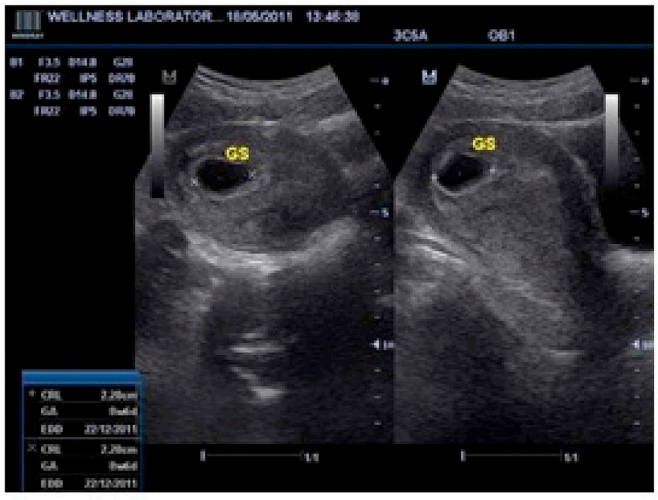

(c)

Fig. 5c. Original image.

(d)

Fig. 5d. Filtered image contains the perceptual quality of the original image.

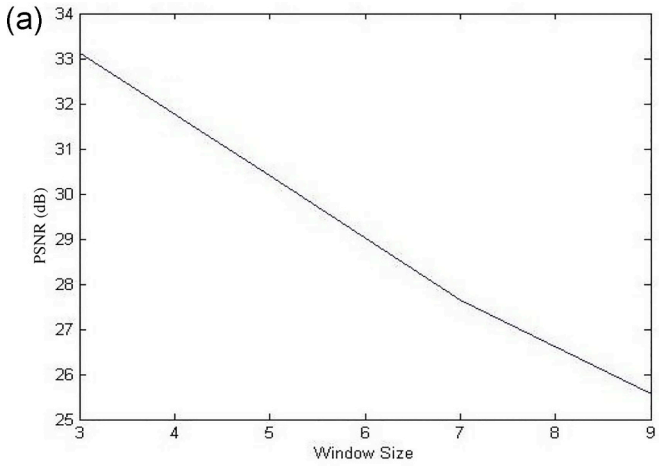

Fig. 6a. Graph of the average PSNR per window size using the median filter.

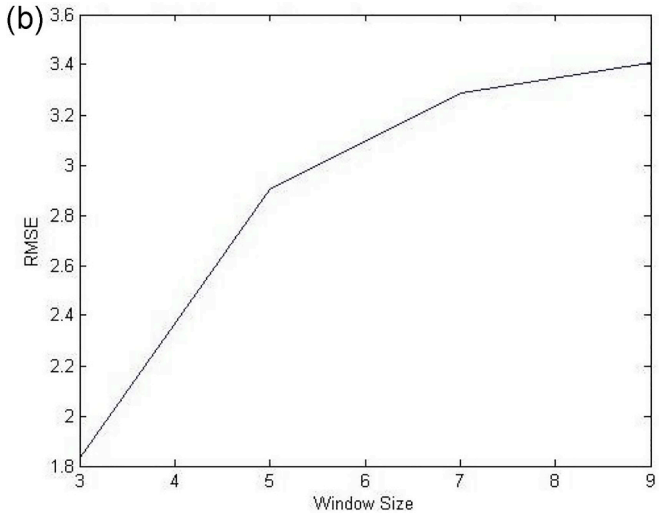

Fig. 6b. Graph of the average RMSE per window size using median filter.

Table 2
DWT of sample ultrasound images for two different scenarios.

Image	Two levels of decomposition (Scenario 1)				Three level decomposition (Scenario 2)			
	Discarded coefficients	PSNR (dB)	RMSE	SSIM	Discarded Coefficients	PSNR (dB)	RMSE	SSIM
Image 1	241553	30.9619	0.5039	0.8732	247213	29.6098	0.6702	0.8010
Image 2	119425	24.1286	0.9927	0.8697	122357	23.8722	1.0225	0.7689
Image 3	97345	27.7495	0.5543	0.8043	101002	27.1934	0.6976	0.7115
Image 4	237033	26.3682	0.8607	0.8323	245293	25.1994	0.8776	0.7932
Image 5	268943	28.0147	0.6240	0.8139	273059	26.8572	0.7392	0.7748
Image 6	203532	27.7434	0.6125	0.8001	230120	27.0192	0.7684	0.7012
Image 7	178320	30.9684	0.5728	0.8510	197192	28.9019	0.7482	0.8291
Image 8	271902	29.0101	0.5049	0.8273	280931	27.0295	0.6937	0.7431
Image 9	202958	29.3920	0.6392	0.8801	220120	27.9484	0.7717	0.7717
Image 10	238520	27.9320	0.6026	0.8490	243212	26.5839	0.7928	0.7928

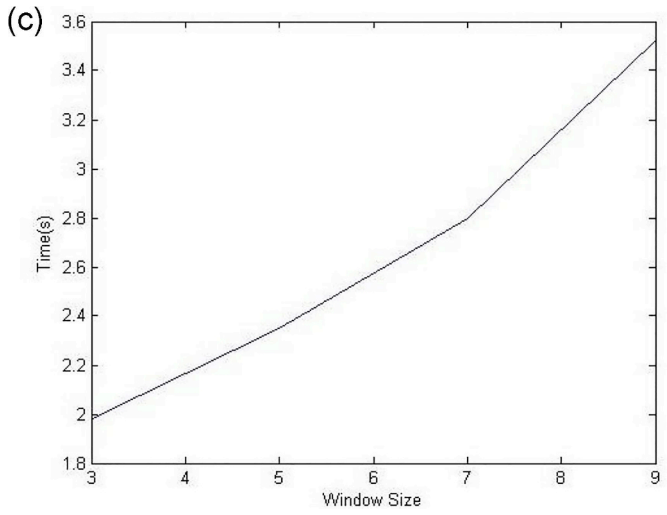

Fig. 6c. Graph of the average time per window size using median filter.

overall preprocessing step. Considering the amount of time needed to compute the median filter, it can be realized from Fig. 5 (c) that as the window size of the median filter increases, the time needed to perform the preprocessing also increases. This is due to the fact that many more pixels are considered when a median is to be found. In the case of a 3×3 dimension, the pixels of interest are nine in number. As the window size increases, more pixels are added up. The extreme case of a 9×9 window size means that for median determination, eighty-one different pixels are considered; hence the increase in computation time.

4.2. DWT operation

After the DWT is performed on the filtered image and a threshold is applied to the resulting coefficients, the performance of the application of the threshold on the coefficients is evaluated. Two different scenarios are considered; a two-level decomposition and a three-level decomposition. After the transformation, all coefficients that fall below the threshold are set to zero. Table 2 shows the results of PSNR and RMSE of sample reconstructed images from DICOM samples. The number of discarded coefficients is also displayed. The total samples used consist of 361 images of CT modality and 135 of MRI modality. Some additional 251 images consisting of 170 Ultrasound, 50 X-Ray and 21 CT from hospital were also added for processing and validation.

The results conclude that discarding some coefficients has not caused too much noise in the image. The quality of the image is thus still intact. The high PSNR values show this effect. Of particular interest is the number of coefficients discarded. This increases the chances of having many zero-coefficients chained together. Increasing the number of levels increases the number of discarded coefficients.

4.3. Vector quantization and encoding

Experiments performed in this stage considered different codebook sizes and different window sizes. For each of the four images, a test is performed to assess the efficiency of the quantizer with varying codebook and window sizes. Further compression by the Huffman encoding algorithm shows the outstanding results in Figs. (7 – 9). The graphs also indicate the compression ratios per widow size per codebook size. The peak signal to noise ratio (PSNR) and the root mean square error (RMSE) provide a substantial amount of the quality of the image formed.

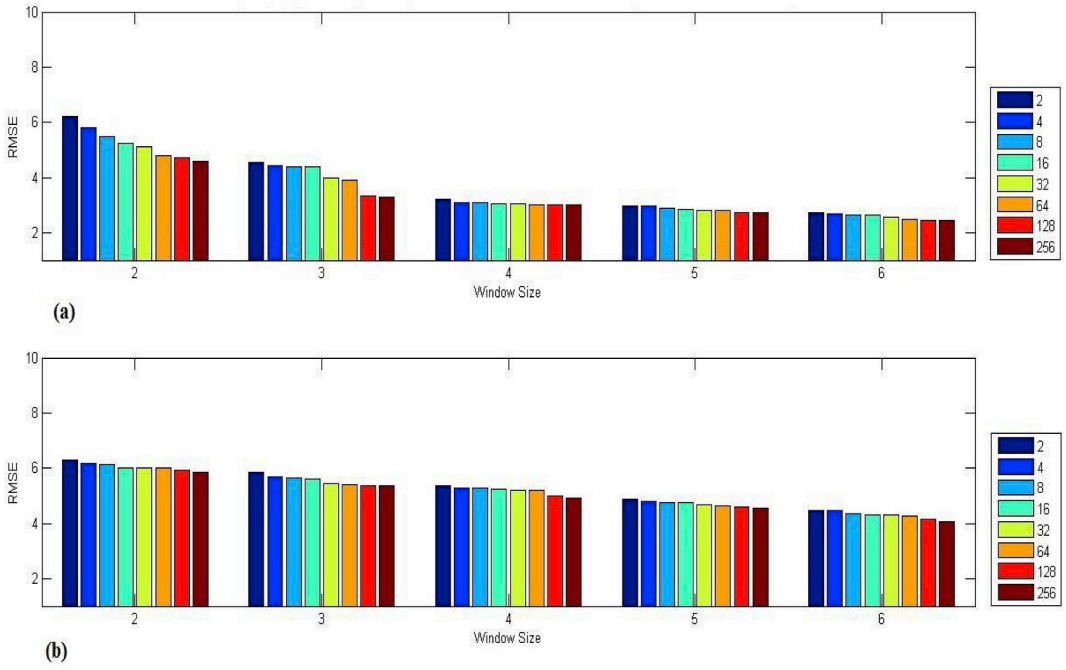

Fig. 7. Graph of average RMSE per window size for different codebook sizes ((**a**) Scenario 1 and (**b**) Scenario 2).

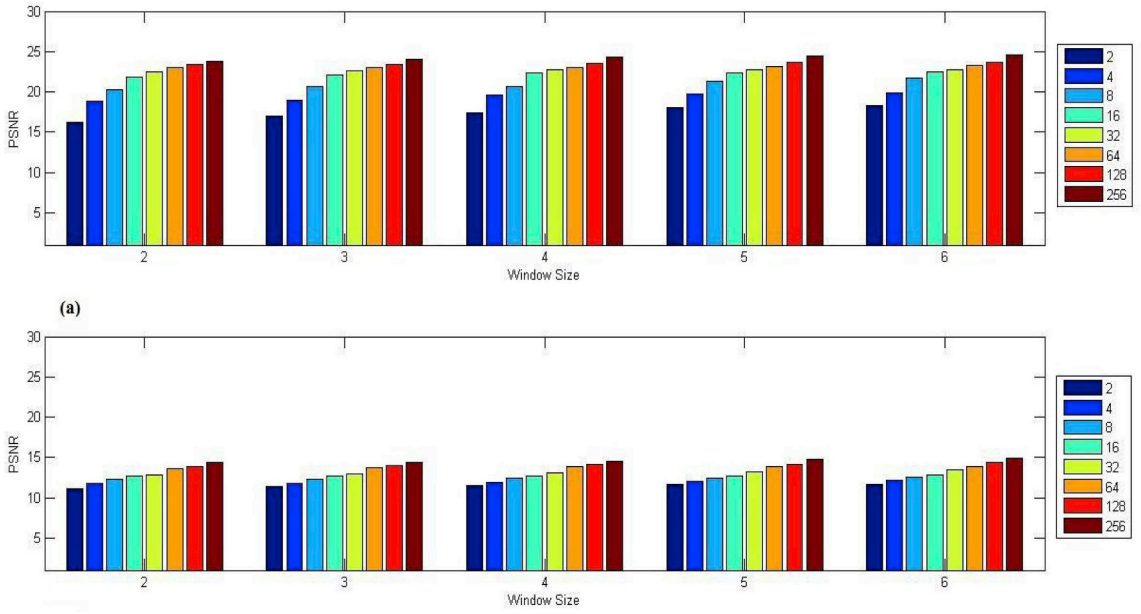

Fig. 8. Graph of average PSNR per window size for different codebook sizes. (a. Scenario 1 and b. Scenario 2).

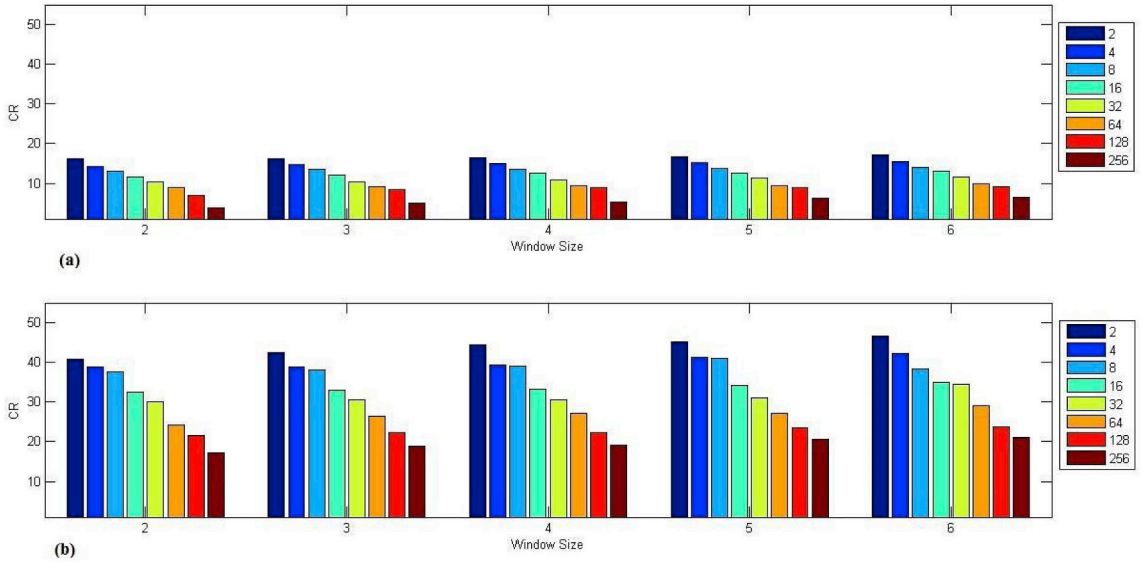

Fig. 9. Graph of average compression ratio per window size for different codebook sizes ((a) Scenario 1 and (b) Scenario 2).

As codebook size increases, it can be noticed that there is a significant decrease in the RMSE.

The following are some of the highlights of the images produced from the experiments for both scenarios. The samples shown here in Fig. 8 and Fig. 10 reemphasized the fact that a higher codebook size is needed to maintain image quality and therefore a suitable choice for the hybrid algorithm, since image quality is critical in medical imaging (see Fig. 9).

Sample results of different image types and sizes after compression are shown in Table 3.

4.4. Performance evaluation

The performance of the proposed technique is compared directly to other methods with similar image set-up. The result as displayed in Table 4 indicates clearly that the proposed method outperforms the

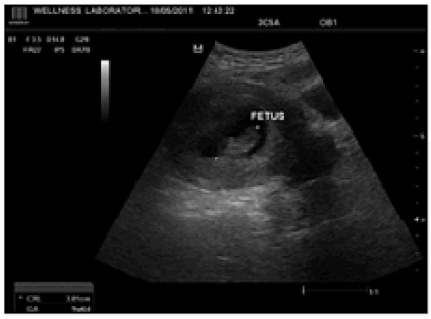

Original image

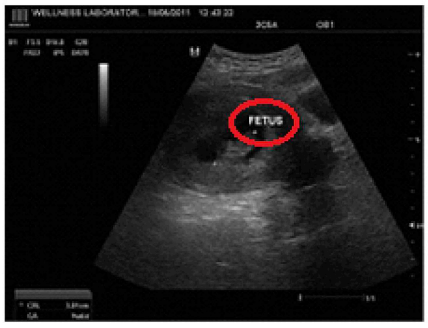

Scenario 1 (***a***): Codebook Size: 2, window size: 3x3; PSNR: 17.79, RMSE: 5.38, CR: 14.40

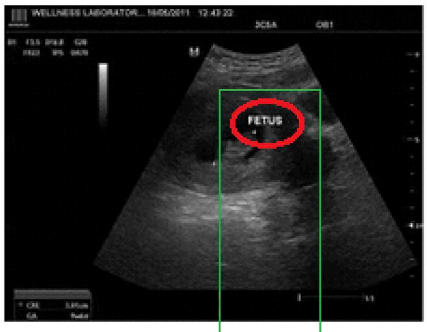

Scenario 1 (***b***): Codebook Size: 256, Window Size: 3x3; PSNR: 24.79 RMSE: 2.94, CR: 7.40

Scenario 2 (***a***): Codebook Size: 2, Window Size: 3x3; PSNR: 11.39, RMSE: 8.94, CR: 43.68

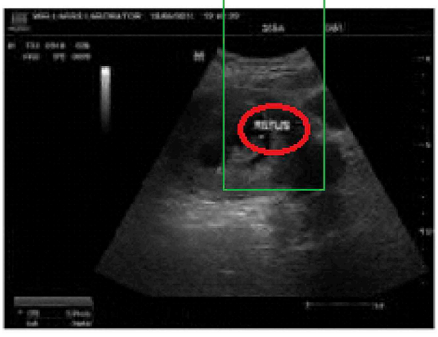

Scenario 2 (***b***): Codebook Size: 256, Window Size: 3x3; PSNR: 13.81, RMSE: 5.35, CR: 19.50

Fig. 10. Sample decompressed images after application of the hybrid algorithm.

Table 3
Results of compression of Case 1 and Case 2 (Codebook size: 256).

Image	Size	Capacity (Original Image in MB)	Case 1: Codebook size: 256				Case 2: Codebook size: 256			
			Capacity (Compressed image in KB)	CR	PSNR (dB)	RMSE	Capacity (Compressed image in KB)	CR	PSNR (dB)	RMSE
Image 1	800 × 600	3.66	506.76	7.40	24.79	2.94	192.30	19.50	13.81	5.35
Image 2	800 × 600	3.66	482.01	7.78	23.62	3.00	171.55	21.86	14.44	4.31
Image 3	800 × 600	3.66	529.66	7.09	23.34	3.88	175.23	21.40	14.09	4.27
Image 4	800 × 600	3.66	537.25	6.98	24.71	2.64	179.08	20.94	13.91	4.13

Table 4
Performance comparison of same images under different methods.

Technique	Image Type	Compression Metric			
		PNSR (dB)	SSIM	CR	MSE
ROI Based Medical Image Compression for Telemedicine Application [26]	MR DICOM samples	53.27168	NA	89.6005	1.03736
Proposed		60.1640	NA	90.305	1.00125
Wavelet Based Medical Image Compression For Telemedicine Application [27]	MR DICOM samples	37.32	NA	87.50	57.50
Proposed method		43.31	NA	91.25	46.49

Table 5
Description of datasets used in Table 6.

Image Type	Resolution (w/h/d in px)	Dynamic range (bpp)	0-order entropy (bpp)	Pixel pitch (w/h/d in mm)	Content
CT1	512/512/201	12	8.35	1.000/1.000/1.000	Axial thoracic lung scan
CT2	512/512/242	12	9.32	1.000/1.000/1.000	Axial thoracic lung scan
CT3	512/512/75	12	8.98	1.000/1.000/1.000	Axial spiral arterial scan
CT4	512/512/100	12	7.37	1.000/1.000/1.000	Axial scan of female cadaver (slices 100–199)
CT5	512/512/672	12	6.62	0.977/0.977/2.500	Axial scan of human cadaver (full scan)
CT6	512/512/44	12	8.10	0.660/0.660/5.000	Helical scan of normal chest and mediastinum
MRI1	432/432/250	12	5.13	0.579/0.579/0.579	Normal brain at 3.0 T
MRI2	256/256/200	12	6.15	0.860/0.860/0.800	Normal brain at 1.0 T
MRI3	256/256/100	12	6.41	0.977/0.977/2.000	Normal brain at 1.5 T
US1	500/244/201	8	7.05	NA	Fetal spine ultrasound
US2	352/242/136	8	7.27	NA	Fetal brain ultrasound

Table 6
Summary of lossy compression comparison of two methods.

Image	Wavelet based volumetric medical image compression [28] (HEVC-RA)		Proposed method	
	Bit-rate (bpp)	PSNR (db)	Bit-rate (bpp)	PSNR (db)
CT1	1.88	61.35	1.63	63.71
CT1	1.65	60.53	1.50	62.66
CT2	2.89	52.79	2.68	58.04
CT2	2.00	48.02	1.79	52.32
CT3	1.68	61.94	1.45	66.09
CT3	1.51	60.21	1.28	65.44
CT4	1.27	63.28	1.01	67.84
CT4	1.18	62.59	1.03	64.11
CT5	0.86	66.60	0.61	71.27
CT5	0.86	66.52	0.63	70.76
CT6	2.00	60.17	1.91	65.40
CT6	1.79	58.81	1.70	63.26
MRI1	1.71	63.31	168	68.64
MRI1	1.49	61.77	1.42	65.17
MRI2	2.55	59.30	2.56	61.25
MRI2	1.94	55.67	1.83	57.37
MRI3	2.33	57.26	2.31	58.04
MRI3	1.81	53.74	1.92	53.87
US1	2.90	49.86	2.77	57.51
US1	2.00	44.24	1.92	50.02
US2	2.83	47.38	2.87	55.38
US2	2.00	41.99	1.98	47.53

others. The quality of the compressed image is also compared in Table 6 with another result in terms of the PNSR. The description of the data sets for Table 6 is shown in Table 5.

Fig. 11 shows sample reconstructed images from DICOM and datasets in Table 6.

5. Conclusion

In this paper, a hybrid of Discrete Wavelet Transform (DWT) and Vector Quantization (VQ) is proposed to complex medical imaging and retain the diagnostic content as well. A thresholding approach is introduced between the two major techniques, and wavelet coefficients are generated. This value that falls below the specified threshold is zeroed out to increase the likelihood of obtaining a chain of zeroes, which increases the efficiency of the quantizer. A default codeword composed of zeroes is injected into the codebook to the desired codebook size. The thresholding has a negligible impact on the quality of the restored image. The final codebook is utilized to encode the coefficients, and it is finally encoded through Huffman techniques. The best combination for the hybrid technique is achieved when two levels of DWT are applied prior to quantization.

The proposed hybrid technique shows outstanding performance when compared with other methods. Further improvement of the study will investigate the effect of compressions using a multiwavelet decomposition technique. Another improvement will involve the inclusion of physical design of filters.

Disclosures

There are no conflicts of interest, financial or otherwise to be declared by the authors.

Conflicts of interest

We declare that we don't have any conflict of interest with any third party.

Ethical statement

We confirm that this work is original and has not been published

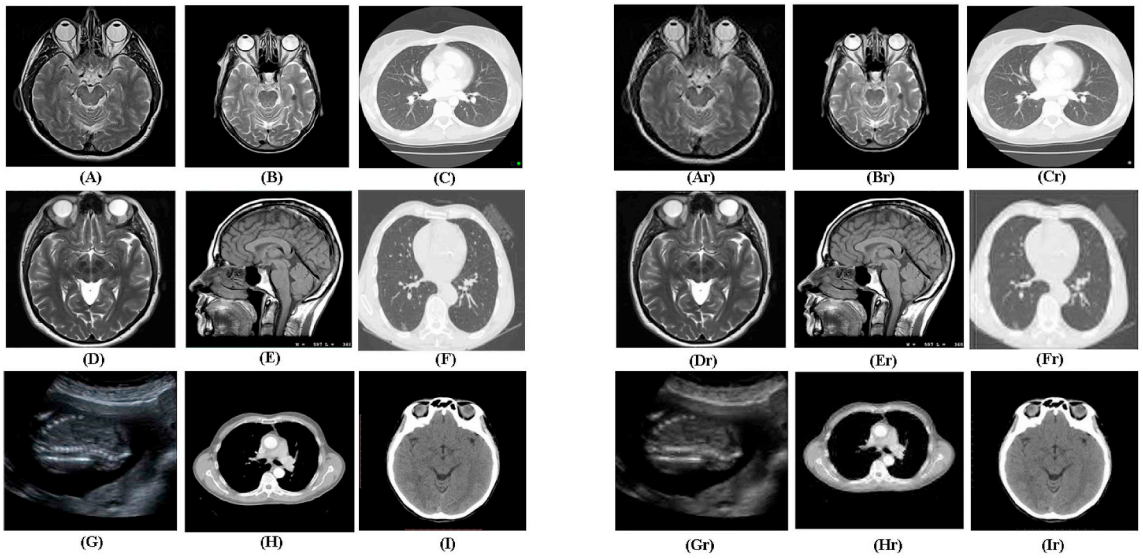

Fig. 11. Selected images from DICOM and images in Table 6. (A) MRI brain at 3.0T, (B) MRI image of brain, (C) Axial lung, (D) MRI brain, (E) MRI of head showing the full brain from top, (F) Lung cancer diagnostic image, (G) Ultrasound festal spine (H) CT chest scan, (I) MRI normal brain at 1.5T. The reconstructed images are: (Ar) for reconstructed of (A) etc.

elsewhere nor is it currently under consideration for publication elsewhere.

Acknowledgments

Special thanks to the Department of Radiology, Korle-Bu Teaching Hospital, Accra, for providing the images used for this project. The authors have nothing to declare as conflicts of interest.

Appendix A. Supplementary data

Supplementary data to this article can be found online at https://doi.org/10.1016/j.imu.2019.100183.

References

[1] Smith-Bindman R, Miglioretti DL, Johnson E, Lee C, Feigelson HS, Flynn M, Greenlee RT, Kruger RL, Hornbrook MC, Roblin D, Solberg LI. Use of diagnostic imaging studies and associated radiation exposure for patients enrolled in large integrated health care systems. Jama 2012;307:2400–9.
[2] Smith-Bindman R, Miglioretti DL, Larson EB. Rising use of diagnostic medical imaging in a large integrated health system. Health Aff 2008;27:1491–502.
[3] Jones T, Townsend DW. History and future technical innovation in positron emission tomography. J Med Imaging 2017;4:011013.
[4] Reinhard E, Heidrich W, Debevec P, Pattanaik S, Ward G, Myszkowski K. High dynamic range imaging: acquisition, display, and image-based lighting. Morgan Kaufmann; 2010.
[5] Al-Qershi OM, Khoo BE. High capacity data hiding schemes for medical images based on difference expansion. J Syst Softw 2011;84:105–12.
[6] Hashem IAT, Yaqoob I, Anuar NB, Mokhtar S, Gani A, Khan SU. The rise of "big data" on cloud computing: review and open research issues. Inf Syst 2015;47:98–115.
[7] House MJ, Bangma SJ, Thomas M, Gan EK, Ayonrinde OT, Adams LA, Olynyk JK, St Pierre TG. Texture-based classification of liver fibrosis using MRI. J Magn Reson Imaging 2015;41:322–8.
[8] El Khaddar MA, Harroud H, Boulmalf M, Elkoutbi M, Habbani A. Emerging wireless technologies in e-health trends, challenges, and framework design issues. IEEE international conference on multimedia computing and systems (ICMCS). 2012. p. 440–5.
[9] Spaulding J, Noda H, Shirazi MN, Kawaguchi E. BPCS steganography using EZW lossy compressed images. Pattern Recogn Lett 2002;23:1579–87.
[10] Mallat SG. A theory for multiresolution signal decomposition: the wavelet representation. IEEE Trans Pattern Anal Mach Intell 1989;11:674–93.
[11] Vetterli M, Herley C. Wavelets and filter banks: theory and design. IEEE Trans Signal Process 1992:40.
[12] Daubechies I. Ten lectures on wavelets. Philadelphia: Society for Industrial and Applied Mathematics; 1992.
[13] Reichel J, Menegaz G, Nadenau MJ, Kunt M. Integer wavelet transform for embedded lossy to lossless image compression. IEEE Trans Image Process 2001;10:383–92.
[14] Yung-Gi W, Shen-Chuan T. Medical image compression by discrete cosine transform spectral strategy. IEEE Trans Inf Technol Biomed 2001;5:236–43.
[15] Shannon CE. A Mathematical theory of communication. Bell Syst Tech J 1948;27:379–423.
[16] Patel TS. Image compression using DWT and vector quantization. Int J Innov Res Comput Commun Eng 2013;1:653.
[17] Mohammed AA, Hussein JA. Efficient hybrid transform scheme for medical image compression. Int J Comput Appl 2011;27:16–20.
[18] Janet J, Mohandass D, Meenalosini S. Lossless compression techniques for Medical images in Telemedicine. Advances in telemedicine: technologies, enabling factors and scenarios. InTech; 2011.
[19] Lal M, Kaur L, Gupta S. Speckle reduction with edge preservation in B-scan breast ultrasound images. Int J Image Graph Signal Process 2016;8:60.
[20] Yousuf MA, Nobi MN. A new method to remove noise in magnetic resonance and ultrasound images. J Sci Res 2010;3:81.
[21] Lu CT, Chou TC. Denoising of salt-and-pepper noise corrupted image using modified directional-weighted-median filter. Pattern Recogn Lett 2012;33:1287–95.
[22] Betz S, Bhagat N, Murhy P, Stengler M. Wavelet based image compression–analysis of results.
[23] Sunil H, Hiremath SG. A combined scheme of pixel and block level splitting for medical image compression and reconstruction. Alexandria Eng J 2018;57:767–72.
[24] Gupta R, Mehrotra D, Tyagi RK. Comparative analysis of edge-based fractal image compression using nearest neighbor technique in various frequency domains. Alexandria Eng J 2018;57:1525–33.
[25] Wang Z, Simoncelli EP, Bovik AC. Multiscale structural similarity for image quality assessment. IEEE Thirty-Seventh Asilomar Conference on Signals, Systems & Computers. 2003. p. 1398–402.
[26] Kaur M, Wasson V. ROI based medical image compression for telemedicine application. Procedia Computer Science 2015;70:579–85.
[27] Korde NS, Gurjar DA. Wavelet based medical image compression for telemedicine application. Am J Eng Res 2014.
[28] Bruylants T, Munteanu A, Schelkens P. Wavelet based volumetric medical image compression. Signal Process Image Commun 2015;31:112–33.